Elliptical normal modes and stop band reconfiguration in multimode birefringent one-dimensional magnetophotonic crystals

Ashim Chakravarty, Miguel Levy,* Amir A. Jalali, and Zhuoyuan Wu
Department of Physics, Michigan Technological University, 1400 Townsend Drive, Houghton, Michigan 49931 USA

Alexander M. Merzlikin
Institute of Theoretical and Applied Electromagnetics, Russian Academy of Sciences Moscow 125412, Russia
(Received 24 May 2011; published 12 September 2011)

This study examines photonic stop band reconfiguration upon magnetization reversal in multimode elliptically birefringent Bragg filter waveguides. Magnetization reversal in longitudinally magnetized magneto-optic waveguides affects the character of the local orthogonal elliptically polarized normal modes, impacting the filter's stop band configuration. Unlike the standard case of circular birefringence in magneto-optic media, opposite helicity states do not transform into each other upon magnetization reversal for a given propagation direction. Rather, helicity reversals yield new and different normal modes with perpendicularly oriented semimajor axes, corresponding to a north-south mirror reflection through the equatorial plane of the Poincaré sphere. For asymmetric contradirectional coupling between different-order waveguide modes in multimode magnetophotonic crystals, this symmetry breaking, namely, the obliteration of normal modes upon magnetization reversal, allows for strongly reconfigured stop bands, through the hybridization of the elliptically polarized states. The effect of Bloch mode reconfiguration on the stop band spectral profile contributes to the magnetic response of the filter. In such elliptically birefringent media, input polarization helicity reversal also becomes a powerful tool for optical transmittance control. Both magnetization and helicity reversals can thus serve as useful tools for the fabrication of on-chip magnetophotonic crystal switches.

DOI: 10.1103/PhysRevB.84.094202 PACS number(s): 42.70.Qs, 78.20.Ls, 42.82.Et, 75.50.Gg

I. INTRODUCTION

Photonic crystals fabricated in magneto-optic media have been the subject of numerous studies in recent years. The enhancement of Faraday rotation in one-dimensional layered stacks with resonant cavities was reported in Refs. 1–4. Other authors have studied the band dispersion of photonic crystals containing magnetically ordered materials,[5] and electromagnetic unidirectionality in periodic magnetic stacks and two-dimensional magnetophotonic crystals.[6,7] Wang and Lakhtakia explored magnetically controllable band gaps in one-dimensional helicoidal magnetophotonic crystals.[8] One-way edge modes analogous to quantum Hall edge states in two-dimensional photonic crystals in gyrotropic media were investigated by Haldane and Raghu and other authors.[9–11] Magnetization-induced second-harmonic generation in magnetophotonic crystals was studied by Murzina *et al.*[12] Levy *et al.* reported on flat-top response in multiple resonator one-dimensional magnetophotonic crystals[13] and large polarization rotations in waveguide nonreciprocal Bragg systems.[14–16] They also studied band gap formation, local normal mode coupling, and Bloch states in birefringent magnetophotonic periodic stacks.[17–20] Degenerate band gap periodic magneto-optic systems were analyzed in Ref. 21, while applications of magnetophotonic waveguide Bragg structures to sensors and switches were reported in Refs. 22 and 23.

Among the properties of photonic crystals, the dynamic tuning of their optical response is of particular interest because such dynamic control would enhance the functionality of photonic crystal-based devices. Tunability has been explored through electrical,[24–29] magnetic,[8,29–32] thermal,[30,33] and mechanical control;[34] through immersion in coherent atomic gases,[35] and through variations in the angle of incidence of the optical beam.[36] Magnetic tunability studies have consisted of theoretical band gap analysis focusing on dielectric permittivity or magnetic permeability control and their effect on gap width, band gap center wavelength,[8,29,31,32] and the effect of magnetic fields on the superconducting state in photonic crystals composed of copper oxide high-temperature superconductors.[30] Such magnetophotonic stop band manipulation is particularly interesting as it may have important technological implications for fast optical switching given the extremely fast magnetic response of magneto-optic media. Recent work has shown 40 fs magnetization switching effects.[37]

Here, we discuss and experimentally demonstrate a different mechanism of stop band magnetic tuning particularly suited to multimode one-dimensional magneto-optic waveguides and applicable to integrated on-chip devices. The essential cause of the effect can be traced to normal mode helicity reversals in intermodal contradirectional coupling between different mode orders. The effect is not due to band gap tuning per se but to mode conversion and mode hybridization upon helicity reversals under asymmetric contradirectional coupling conditions. Some degree of Bloch mode reconfiguration does take place, as discussed in Sec. IV, also impacting the stop bands. Large stop band detuning to magnetization and helicity reversals, applicable to controlled optical switching, are demonstrated below for high-order waveguide mode back reflection.

We address this question through an examination of Bragg reflection in elliptically birefringent waveguide media. Elliptical birefringence arises naturally in magneto-optic waveguides due to the combined effects of magneto-optic gyrotropy and shape anisotropy.[14,15,17,19,20] Stress birefringence due to

lattice mismatch between waveguide film and substrate also contributes to the effect.

We show that it is possible to induce significant changes in the stop band spectral dispersion in elliptically birefringent multimode waveguides through hybridized coupling between different forward- and backward-propagating elliptically polarized waveguide modes. The reasons behind these phenomena are discussed below. This stop band reconfiguration is traced to the transmutation of elliptical normal modes into hybrid modes, through their effect on mode propagation in the waveguide.

Normally, waveguide response is examined in terms of transverse electric (TE) and transverse magnetic (TM) modes. In the absence of longitudinal magnetization or gyrotropy, these are normal modes, as each maintains its polarization state as the wave propagates down the guide. However, optical gyrotropy couples TE and TM modes so that they are no longer normal modes. A magnetic bias along the direction of the light propagation in such waveguides activates the gyrotropy thus coupling TE and TM modes and rendering these no longer eigenmodes of the wave equation.

However, elliptically polarized inputs can be shown to generate normal modes in elliptically birefringent waveguides. In other words, once launched into the waveguide, they can be shown to propagate with minimal change to their polarization state. It is in this sense that we speak of elliptically polarized normal modes.

The simultaneous presence of shape anisotropy, lattice mismatch strain, and magnetic anisotropy establishes elliptical birefringence, where opposite-helicity states advance at different speeds through the guide. Generally, the above conditions lead to different diagonal components in the relative permittivity matrix and semimajor axes of the elliptical modes aligning with the directions of transverse electric and transverse magnetic polarizations.[17,20]

Of particular note in our treatment is the stop bands formed as a result of asymmetric contradirectional coupling between different-order forward- and backward-propagating elliptical waveguide modes. As a result, a magnetization reversal in the longitudinal direction completely changes the character of the normal modes in the photonic crystal. Normal modes for any given order differ in their elliptical polarization state. That means that, except for the case of circular polarization, the directions of their semimajor axes are different. Upon magnetization reversal and for a given semimajor axis orientation of the normal mode polarization ellipse, the helicity of that normal mode gets reversed. We study the effect of this normal-mode helicity reversal on the stop band configuration of the magnetophotonic Bragg filter.

Below, we examine these changes from normal to hybrid modes upon magnetization reversal and their impact on stop band magnetic tuning. Elliptical birefringence differs essentially from circular birefringence (Faraday effect) in that a magnetization reversal renders normal modes into hybrid modes in the former but not in the latter case and has a profound effect on stop band tuning.

In addition, we discuss the effects of mode conversion and actual band gap tuning on the stop band reconfiguration. It is shown that changes in Bloch mode configuration upon magnetization reversal produce changes in transmittance and stop band spectra; however, these are small in comparison with those brought about by input polarization changes.

This article is divided into three sections after this introduction. Section II presents a theoretical discussion of electromagnetic wave propagation in birefringent magneto-optic media. Following prior treatments based on stack-model approximations to magneto-optic Bragg filters, we put forth expressions for elliptically polarized normal modes and Bloch states. These models perform extremely well as shown in a subsequent section comparing experimental and theoretical results. Our experimental approach is presented in Sec. III, labeled experimental background. Elliptically polarized states are launched into the magneto-optic waveguide and the one-dimensional magneto-optic Bragg reflector, and the transmittance and output polarization states are analyzed. Stokes parameter methodology and rotating polarizer analysis are utilized for this purpose. The experimental response of the elliptically birefringent magnetophotonic crystals is discussed in Sec. IV labeled results and discussion. A comparison with the theoretical predictions based on the model discussed in Sec. II is presented and shown to give remarkably good agreement, in support of the asymmetric scattering model and the helicity dependence of magneto-optic stop band tuning. The conditions for strong magneto-optic control of the stop band are analyzed.

II. THEORETICAL BACKGROUND

The electromagnetic wave equation in a birefringent magneto-optic medium is given by[17,20]

$$\left(k_0^2\tilde{\varepsilon} - k^2\mathbf{I} + \mathbf{kk}\right)\mathbf{E}_0 = 0, \tag{1}$$

where $\mathbf{E}_0$ is the plane wave amplitude, $\mathbf{kk}$ is a dyadic product of the wave vector, $\mathbf{I}$ is the 3×3 identity matrix, and $k_0^2 = \omega/c$, c is the speed of light, and ω is its angular frequency. The relative permittivity matrix, $\tilde{\varepsilon}$ of the birefringent magneto-optic crystal magnetized along the direction of light propagation (z direction) has the form:

$$\tilde{\varepsilon} = \begin{pmatrix} \varepsilon_{xx} & \pm ig & 0 \\ \mp ig & \varepsilon_{yy} & 0 \\ 0 & 0 & \varepsilon_{zz} \end{pmatrix}. \tag{2}$$

The above relation assumes no absorption of light in the medium with ε_{xx}, ε_{yy}, ε_{zz} and g having real values. From Eq. (2), the condition for elliptical birefringence is given by $\varepsilon_{xx} \neq \varepsilon_{yy}$. The nonreciprocal gyrotropy is parameterized by the off-diagonal components $\pm ig$ in the relative permittivity matrix.

The above formulation applies to a uniform medium. An exact treatment of a dielectric waveguide would require solving the wave equation separately in the waveguide core as well as in the cladding and then matching boundary conditions. Here, we use an alternative approach for the expressed purpose of obtaining expressions for the polarization of the elliptical eigenmodes. A layered stack (Fig. 1) is used to model the transmittance and polarization response of the magneto-optic photonic crystal in conjunction with experimentally extracted waveguide mode parameters, as described in this section.

The mode indices for all allowed TE and TM waves in the waveguide are measured experimentally using a

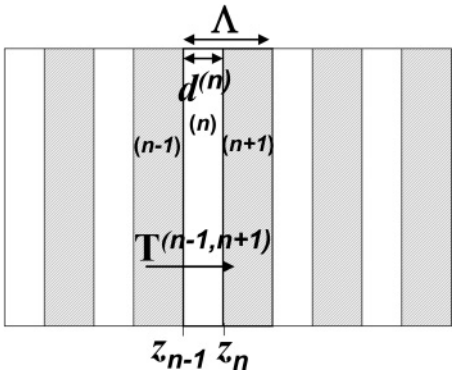

FIG. 1. Layered stack used for modeling the transmittance for intermodal scattering. The model makes use of a bilayer unit cell with period Λ. Propagation is in the z direction, normal to the layer planes.

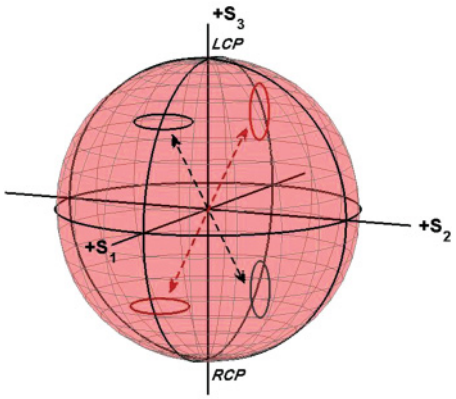

FIG. 2. (Color online) Poincaré sphere showing complementary elliptical normal modes for a given propagation direction, joined by either of the double-tipped arrows.

prism-coupling technique and are also tested against the Bragg condition in the Bragg filter in transverse magnetization. Transverse magnetization condition allows us to determine mode indices in the absence of TE/TM coupling for linearly polarized inputs. Upon longitudinal magnetization, TE and TM modes couple as a result of the Faraday effect (nonreciprocal gyrotropy).

For each TE/TM pair of a given mode order, the wave is treated as propagating in an anisotropic material having refractive indices for transverse horizontal and vertical polarizations equal to those of the given TE and TM waveguide modes in transverse magnetization. The elliptical polarization and mode indices for longitudinal magnetization are obtained by solving the dielectric permittivity eigenvalue problem in the presence of nonreciprocal gyrotropy. Thus, we approximate the diagonal components ε_{xx} and ε_{yy} of the relative permittivity matrix in Eq. (2) with the relative permittivity scalars (the squares of the mode indices for transverse magnetization) of the corresponding fundamental or high-order TE and TM modes, respectively. This approach works extremely well in predicting the elliptical normal modes of the waveguides, as can be seen in the results and discussion section below.

By solving the wave equation Eq. (1), upon normal incidence of a monochromatic plane wave propagating parallel to the z axis for the system in Eq. (2), the parameterized elliptical eigenmodes and their phase speeds $v_\pm$ are given by:[17,20,38]

$$\hat{e}_\pm = \frac{1}{\sqrt{2}} \begin{pmatrix} \cos\alpha \pm \sin\alpha \\ \pm i\cos\alpha - i\sin\alpha \\ 0 \end{pmatrix}, \tag{3}$$

$$\tan(2\alpha) = \frac{\varepsilon_{yy} - \varepsilon_{xx}}{2g}, \tag{4}$$

$$v_\pm = c/n_\pm, \tag{5}$$

$$n_\pm^2 = \bar{\varepsilon} \pm \sqrt{\Delta^2 + g^2}, \tag{6}$$

$$\bar{\varepsilon} = \frac{\varepsilon_{yy} + \varepsilon_{xx}}{2}, \tag{7}$$

and

$$\Delta = (\varepsilon_{yy} - \varepsilon_{xx})/2. \tag{8}$$

Here, $n_\pm$ are referred to as the mode indices of the elliptical eigenmodes. Below, we use these eigenmodes as the eigenmodes of the elliptically birefringent media magnetized in the direction of light propagation. When the direction of magnetization is opposite to the direction of the light propagation, the gyration vector of the media is reversed, and as a result, the helicities of the eigenmodes are also reversed. This makes the relative permittivity matrix in Eq. (2) acquire both positive and negative signs in the nonreciprocal gyrotropic term. Magnetization reversal changes the sign of g in Eq. (4). As a result, α becomes $\frac{\pi}{2} - \alpha$, and the eigenmodes of the wave Eq. (1), for the reversed magnetization, are parameterized as

$$\hat{e}_\pm^r = \frac{1}{\sqrt{2}} \begin{pmatrix} \pm\cos\alpha + \sin\alpha \\ -i\cos\alpha \pm i\sin\alpha \\ 0 \end{pmatrix}, \tag{9}$$

where the superscript r indicates helicity reversal of the prior eigenmodes.

Figure 2 plots the effect of magnetization reversal on the normal modes in a Poincaré sphere representation. While circular birefringence with normal modes on the north and south poles results in an interchange of modes, an elliptically birefringent medium acquires different modes for a given propagation direction. Magnetization reversal corresponds to a reflection through the equatorial plane. The effect is equivalent to a time reversal operation with the original modes reversing their helicities.

The stop bands in magneto-optic Bragg filters have been discussed by Levy *et al.* in several publications[2,14,15,17,19,20] and have been shown to obey the Bragg condition $\lambda = (n_f + n_b)\Lambda$, where λ is the wavelength in vacuum, n_f and n_b are the mode indices of the forward- and backward-propagating modes, and Λ is the grating period. Multiple stop bands form as a result of the contradirectional coupling of fundamental forward-propagating modes to different back-reflected waveguide mode orders, as shown in Fig. 3. These multiple stop bands appear because the optical wave incident in the grating region and the back-reflected wave satisfy the phase matching condition $\boldsymbol{\beta}_{\text{back}} = \boldsymbol{\beta}_{\text{incident}} + q\mathbf{K}$. Here, $\boldsymbol{\beta}_{\text{incident}}$ and $\boldsymbol{\beta}_{\text{back}}$ are the propagation vectors of the incident and back-reflected waves, respectively; $\mathbf{K}$ is the grating vector pointing in the direction of the ridge waveguide axis and related to the grating

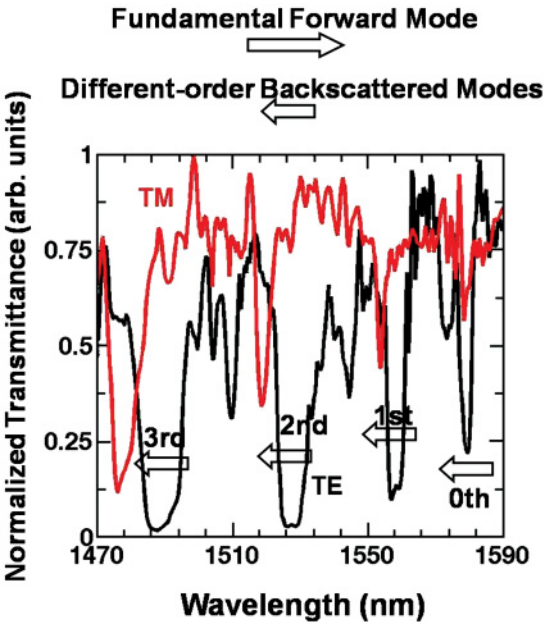

FIG. 3. (Color online) Normalized transmittance of a waveguide Bragg reflector fabricated in a 2.7-μm-thick $Bi_{0.8}Gd_{0.2}Lu_{2.0}Fe_5O_{12}$ film. The spectrum displays several stop bands corresponding to back reflections into different-order modes for TE and TM fundamental mode inputs. The spectra are taken for transverse magnetization in order not to mix the modes.

period Λ by $|\mathbf{K}| = 2\pi/\Lambda$. Here, $q = 0, \pm1, \pm2, \ldots$ is the order of the coupling. The vectors $\boldsymbol{\beta}_{\text{incident}} + q\mathbf{K}$ are called space harmonics and are produced as a result of the spatial modulation of the dielectric permittivity in the grating region. Notice that waveguide mode propagation depends not only on the permittivity of the waveguide core but also on the permittivity of the cladding and cover so that a relief grating introduces spatial modulation. The stop bands then form when the space harmonics match the propagation vectors of allowed waveguide modes traveling in the backward direction. Several stop bands occur because our waveguides are multimode. The order of the coupling is -1, that is, first-order contradirectional coupling.[39]

The modal character of the forward-traveling and back-reflected waves has been determined by an analysis of the stop band spectrum. This information was supplemented by beam-propagation simulations to estimate that more than 90% of the coupled optical power in the forward direction is in the fundamental mode. A commercial optical-waveguide simulation package distributed by RSoft Design was used for this purpose. Back-reflected modes have different propagation vectors $|\beta_b^{(m)}| = \frac{2\pi}{\lambda} n_b^{(m)}$, where m is the mode order and $n_b^{(m)}$ its effective refractive index or mode index.[39] These modes satisfy the phase-matching condition $\boldsymbol{\beta}_b = \boldsymbol{\beta}_f - \mathbf{K}$ sequentially, from fundamental back-reflection at the longest-wavelength stop band through first, second, and higher orders towards shorter wavelengths in the stop band spectrum. Figure 3 labels the stop bands according to this trend. Stop band center wavelengths computed from the Bragg condition as well as calculated stop bands based on power transfer efficiency show very good agreement with the experimental data with average departures of 2 nm (0.15%) and less than 5 nm between calculation and experiment. Power transfer efficiency is a function of the phase mismatch $|\boldsymbol{\beta}_b - (\boldsymbol{\beta}_f - \mathbf{K})|$.[39]

Since forward-fundamental and backward-propagating high-order modes have different ellipticities, a magnetization (or time) reversal operation will produce a different transmittance effect through the filter on any given elliptically polarized input if the helicity of the input is maintained. The effect is also true for single-mode circularly birefringent waveguides, but is highly magnified in multimode elliptically birefringent ones, as shown in the section on results and discussion. The contradirectional coupling to highly birefringent elliptically polarized high-order modes is responsible for this effect and leads to strong stop band detuning. This coupling results in Bragg reflection of the forward-propagating light into high-order waveguide modes.

A theoretical model, in the form of a multilayered stack, as shown in Fig. 1, has been developed by Levy *et al.* to describe the formation of multiple stop bands in elliptically birefringent media based on the Floquet–Bloch theorem.[17,19,20] This model is described in detail in Refs. 17,19, and 20. The authors analyze Bloch mode formation based on the analogy between local waveguide normal modes and local modes in each layer of periodic elliptically-birefringent stacks, and examine the formation of optical band gaps in such media. Their work expresses the Bloch mode in an arbitrary layer n of the stack as:

$$\begin{aligned}\mathbf{E}(z,t) = {} & \hat{e}_+^f E_{01} \exp[i\omega n_+^f (z - z_n)/c] \\ & + \hat{e}_+^b E_{02} \exp[-i\omega n_+^b (z - z_n)/c] \\ & + \hat{e}_-^f E_{03} \exp[i\omega n_-^f (z - z_n)/c] \\ & + \hat{e}_-^b E_{04} \exp[-i\omega n_-^b (z - z_n)/c], \end{aligned} \tag{10}$$

where $i = \sqrt{-1}$ for a light wave of frequency ω propagating in the z direction.[17,19,20] Here, the superscripts f and b refer to the forward- and backward-propagating modes, and z_n is the position of the interface. The mode indices $n_\pm^{f,b}$ are assumed to correspond to local waveguide normal modes of opposite helicity. The E_{0j}, $j = 1$–4 are partial-wave amplitude constants with z_n as the location of the interface between two arbitrary layers n and $n + 1$ in the media. The elliptical polarization-state unit-vectors $\hat{e}_\pm^{f,b}$, in the form $\hat{e}_\pm(\alpha^{f,b})$, are the elliptically polarized waveguide normal modes propagating in the forward or backward direction, respectively. Notice that forward- and backward-propagating normal modes have different elliptical polarizations.

Upon magnetization reversal, the intrinsic normal modes of the structure will change so that any polarization state will project over a new basis set of normal modes. Elliptically polarized normal modes $\hat{e}_\pm^{f,b}$, as in the systems under study here, reverse their helicity upon magnetization reversal, changing into the new basis set $\hat{e}_\pm^{r,f,b}$. Bloch states of the periodic structure, expressed as a linear combination of local normal modes [Eq. (10)], also change as a result of these helicity reversals in $\hat{e}_\pm^{f,b}$. The new Bloch modes have the form

$$\begin{aligned}\mathbf{E}(z,t) = {} & \hat{e}_+^{r,f} E_{01} \exp[i\omega n_+^f (z - z_n)/c] \\ & + \hat{e}_+^{r,b} E_{02} \exp[-i\omega n_+^b (z - z_n)/c]\end{aligned}$$

$$+\hat{e}_{-}^{r,f} E_{03} \exp[i\omega n_{-}^{f}(z - z_n)/c]$$
$$+\hat{e}_{-}^{r,b} E_{04} \exp[-i\omega n_{-}^{b}(z - z_n)/c].$$

We refer to this change in Bloch state as Bloch mode reconfiguration. This change results in different coupling strengths for elliptically polarized input light.

A transfer matrix formulation can be built based on this model to calculate the transmittance of the stack, as described in Refs. 17,19, and 20. This transfer matrix approach shows that the magnetic reconfiguration of the photonic crystal itself does contribute to normal-mode stop band spectral reshaping. These results are verified experimentally, as shown below. However, the effect is not as strong as the changes due to input beam polarization conversion in the feeder section before the photonic crystal structure. Strong reconfiguring of the normal-mode stop bands are due to changes in input polarization state in waveguide sections that feed the light to the Bragg reflector. These can be traced to the transmutation of normal modes into hybrid modes upon magnetization reversal and subsequent polarization changes of the beam in the feeder section of the waveguide. Below, we present experimental evidence of stop band reconfiguration, its dependence on magnetization direction, and a comparison with the theoretical predictions of the model described above. Excellent agreement is obtained.

III. EXPERIMENTAL BACKGROUND

A. Sample preparation

In order to study the magnetic tuning of stop bands in elliptically birefringent gyrotropic Bragg filters, waveguide magnetophotonic crystals were patterned on two sets of samples. The first set consisted of 2.7-μm-thick $Bi_{0.8}Gd_{0.2}Lu_{2.0}Fe_5O_{12}$ films having an intrinsic Faraday rotation of 83°/mm. These single-layer bismuth-substituted-rare-earth iron-garnet films were grown by liquid phase epitaxy (LPE) on (100) gadolinium gallium garnet (GGG) substrates. Three samples with multiple waveguides were fabricated in this material and four Bragg filters tested, yielding mutually consistent results. Here, 6-μm-wide 600-nm ridge height waveguide structures were patterned on the film by standard photolithography followed by plasma etching. Also, 200-μm-long 700-nm groove depth Bragg gratings at 343.3-nm period were focused-ion-beam-milled into the ridge waveguides. The photonic crystal structure was positioned approximately 100 μm away from the output facet on two samples and 10 μm away from the input facet on another, on 1.2-μm long ridge waveguides, spanning the length of the sample. Both input and output sides of the waveguide were lapped down to a 0.1-μm grain diamond lapping-film finish.

Refractive index measurements of waveguide modes of the film were done before surface patterning using a prism coupler. Fundamental to third-order TE mode refractive indices measured in the slab were 2.2930, 2.2497, 2.1781, and 2.0765, respectively. Linear birefringence, defined as the difference between TE and TM mode indices, measured for the first four modes were 0.0005, 0.0047, 0.0120, and 0.0210, respectively. Figure 4 shows a scanning electron micrograph of a Bragg filter patterned in one of these $Bi_{0.8}Gd_{0.2}Lu_{2.0}Fe_5O_{12}$ films.

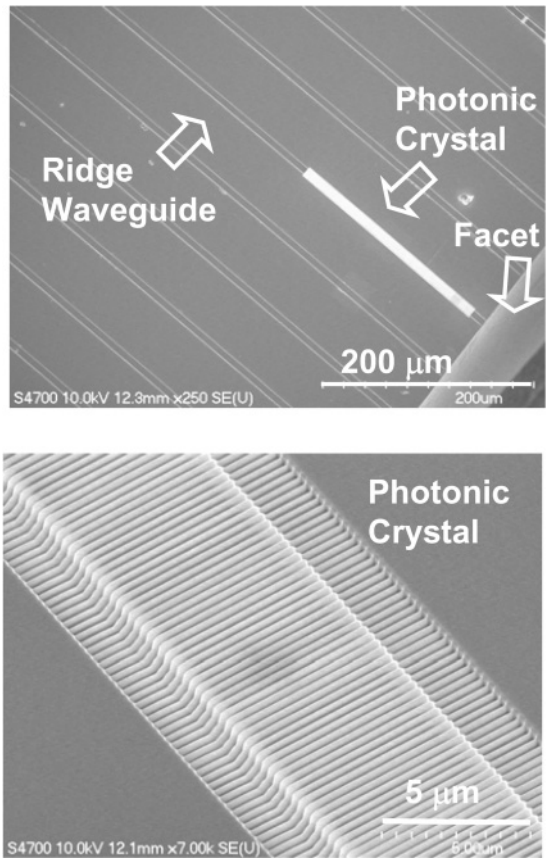

FIG. 4. Scanning electron micrograph of a magnetophotonic crystal waveguide sample fabricated in a 2.7-μm-thick $Bi_{0.8}Gd_{0.2}Lu_{2.0}Fe_5O_{12}$ film.

Stop band tuning tests were also conducted on a second set of (100) LPE on GGG substrate films with composition $Bi_{1.28}Lu_{1.69}Gd_{0.03}Fe_{3.65}Ga_{1.35}O_{12}$ and 2.8-μm thickness ($\pm$0.1 μm). A total of three samples and four Bragg filters were tested for this material with results consistent with the first set. Here, 200-μ m-long photonic crystals with 348-nm period and 700-nm grating groove depths were fabricated in this material. The refractive indices of the first four TE waveguide modes were 2.2805, 2.2425, 2.1784, and 2.0876, respectively. The measured linear birefringence of these waveguide modes were 0.0002, 0.0041, 0.0097, and 0.0169, respectively. The intrinsic Faraday rotation of the film was 95°/mm. Faraday rotation measurements were conducted at 1550-nm wavelength across the thickness of the sample in unpatterned films using a rotating polarizer and phase-sensitive detection.

B. Beam preparation

Elliptically polarized states from a tunable infrared (IR) 1480–1580-nm wavelength fiber-pigtailed source were prepared using a quarter-wave plate, an Agilent 11896A polarization controller, and a linear polarizer. The laser beam goes through the polarization controller and a lensed fiber coupled to the output of the controller. It is then allowed to go through the quarter-wave plate. The latter's fast axis orientation

defines the semimajor axis of the input polarization state. To define the input beam ellipticity (the ratio of the semiminor to semimajor axes amplitudes of the polarization ellipse), a linear polarizer placed after the quarter-wave plate is oriented so that its transmission axis forms an angle $\frac{\pi}{2} - \theta$ relative to the latter's fast axis with $\tan\theta$ equal to the desired ellipticity of the beam. The polarization controller is then adjusted to minimize the intensity of the transmitted light emerging from these two optical components for said configuration. The light coming out of the lensed fiber has the desired polarization.

An ellipticity check is done to confirm the polarization state of the beam by measuring its intensity coming out of the lensed fiber for all 360° orientations of the polarizer axis in steps of 0.1°. The measured ellipticity of a beam is given by the following expression:

$$\text{Ellipticity} = \sqrt{\frac{I_{\min}}{I_{\max}}}, \tag{11}$$

where $I_{\min}$ and $I_{\max}$ are the measured minimum and maximum intensities of the beam. The polarizer angle corresponding to the minimum intensity denotes the semiminor axis orientation of the elliptical polarization state. After the polarization state of the beam is prepared as described above, it is then coupled into the ridge waveguides by butt coupling.

Stokes parameters $S_j (j = 0, 1, 2, 3)$ are used to determine the input beam helicity. Out of these four Stokes parameters S_3 (its sign) determines the helicity of the propagating beam. Experimentally, S_3 is measured using a quarter-wave plate and a linear polarizer. The beam intensity $I(\theta, \phi)$, where θ, ϕ are the linear polarizer axis and quarter-wave plate fast axis orientations, respectively, is first measured just with the linear polarizer at $\theta = 0°$ and 90°. Subsequently, it is measured by inserting the quarter-wave plate ($\phi = 90°$) into the beam path with the linear polarizer set at $\theta = 45°$.[40] Here, S_3 is given by

$$S_3 = I(0°,0°) + I(90°,0°) - 2I(45°,90°). \tag{12}$$

In a Poincaré sphere representation, a beam with polarization coordinate (s_1, s_2, s_3) for normalized Stokes parameters $s_j = \frac{S_j}{S_0}$ is located in the upper hemisphere if S_3 is positive and polarized in the counterclockwise sense as observed from the source or in the clockwise sense as observed from the detector point of view (positive helicity). For a negative value of S_3, the beam carries the opposite (negative) helicity.

C. Measurements

The polarization state of the input beam is prepared to coincide with that of the fundamental normal modes of the waveguide structure. Their ellipticity and helicity are determined using the values of the linear birefringence, the specific Faraday rotation of the film, and Eq. (2). A saturation-magnetic field of 300 Oe collinear with the waveguide axis in the forward and backward directions is used to magnetize the sample.

To confirm that the input beam couples into a normal mode, it is tested on a plain waveguide first before launching it into a Bragg reflector. This test is done to verify that its polarization state remains largely unchanged as the beam propagates down the guide. Light prepared in normal mode polarization states is then launched from the feeder side to the Bragg reflector. Transmittance spectra for fundamental-forward-to-high-order (first, second, and third) as well as to fundamental-backward-propagating-mode stop bands are measured using normal-mode and TE-mode inputs. These measurements are done for parallel and antiparallel directions of the longitudinal magnetic field relative to the beam propagation direction. Normal-mode polarization states are prepared at center wavelength of the TE stop bands with no significant input polarization state departures observed for ±20-nm wavelength detuning away from the center wavelength.

IV. RESULTS AND DISCUSSION

A. Mode conversion in the waveguide feeder section

Our analysis of the normal-mode response in plain waveguides confirms that, unlike other polarization states, normal-mode polarization states remain unchanged as the beam propagates through the medium. Figure 5 plots the polarization response of an elliptical normal mode ($s_3 = 0.48$) and a reversed helicity mode ($s_3 = -0.48$) having the same ellipticity ($|s_3| = 0.48$) before [Fig. 5(a)] and after [Fig. 5(b)] propagating through a typical magneto-optic ridge waveguide fabricated in $Bi_{0.8}Gd_{0.2}Lu_{2.0}Fe_5O_{12}$ and magnetized in the longitudinal direction. Shown are 360° analyzer scans, where 0° and 180° correspond to the orientation of the semiminor axis. Figure 5(b) shows that the reversed helicity mode deviates significantly from the input, whereas the normal mode remains largely unaltered to within experimental accuracy ($\Delta s_3 \leqslant 0.05$).

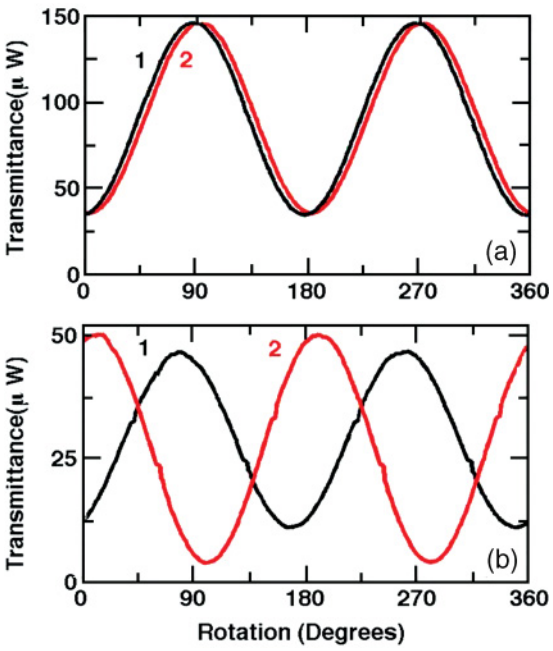

FIG. 5. (Color online) Polarization response for plain waveguide of a normal mode (curve 1) and a reversed-helicity mode (curve 2) having the same ellipticity and semimajor axis orientation. The figure plots polarization analyzer 360° scans, showing (a) overlapping inputs into the waveguide and (b) different outputs after propagating through a 1.2-mm-long waveguide.

Ellipticity is preserved to $\Delta s_3 \leqslant 0.05$ or better. Deviations of less than 8° in semimajor axis orientation over a 1-mm feeder section are routinely recorded for the normal mode. This confirms that normal modes are magnetization-direction and helicity dependent.

B. Photonic crystal stop bands and magnetization reversal

Next, we consider the stop band response to normal modes and reverse-helicity modes. Significant departures are found upon magnetization reversal between opposite helicity inputs on the same photonic band gap structure. These are ascribed to changes in polarization state of the reverse-helicity mode as it propagates down the section of the guide feeding into the Bragg reflector (feeder section). Changes in the stop band spectral shape were also found for Bragg filters fabricated ~10 μm from the input facet. These changes are ascribed to changes in the Bloch mode configuration of the photonic crystal, as discussed below.

Gyrotropic stop bands were studied by launching elliptical normal modes from the feeder side to the photonic crystal, as shown in Fig. 6. This figure displays normal-mode transmittance for a fundamental forward-mode to second-order back-reflected mode stop band (black) for a $Bi_{0.8}Gd_{0.2}Lu_{2.0}Fe_5O_{12}$ film. Plots are shown in absolute units [Fig. 6(a)] and also in units normalized to the transmittance of a plain waveguide without Bragg filter [Fig. 6(b)]. Normalization takes into account spectral changes in input power at the power source. For comparison, we also display here the TE stop band (blue). These results agree with theoretical calculations for normal and TE modes based on the model described in Sec. II and plotted in Fig. 6(c).

A different response is found upon magnetization reversal, as displayed in Fig. 6(d). Here, the mode hybridizes as it is no longer a normal mode, even though the input polarization is the same. This change is due to the conversion of the normal mode into a hybrid mode and its subsequent evolution in the waveguide. Mode conversion into the reverse-helicity normal mode in the waveguide feeder section is almost complete, as the stop band shifts to the one corresponding to that mode. These results agree remarkably well with stop band calculations from the theoretical model described in Sec. II, as shown in Fig. 6(c). Mode conversion and strong stop band reconfiguration was reproducibly observed in all samples tested. This reconfiguration is consistent with the mode conversion to a nearly orthogonal mode in the feeder section (curve 2) in Fig. 5.

Of particular note is the very large spectral detuning of the stop band upon magnetization reversal, as it may have useful applications to optical switching devices. In particular, it should be noted that reconfiguration of the stop band upon magnetization reversal or input-polarization helicity reversal can thus convert a stop band into a pass band, enabling optical switching. Given the demonstrated ultrafast response of magnetic switching,[37] the kind of magnetic stop band tuning discussed here may be a promising route to ultrafast optical on-off devices.

This detuning is a direct consequence of the intermodal back-reflection from fundamental to second-order mode. The large refractive index difference between different-helicity backward-propagating modes is responsible for this detuning. A change in helicity of the normal mode from positive to negative together with a change in magnetization direction restores the original normal-mode spectral response [Fig. 6(e)]. Thus, a change in helicity together with magnetization reversal preserves the normal-mode character of the mode and yields an unchanged stop band. These results are repeatable and have been reproduced in three other samples for the same back-reflected second-order mode and for third-order back-reflected modes.

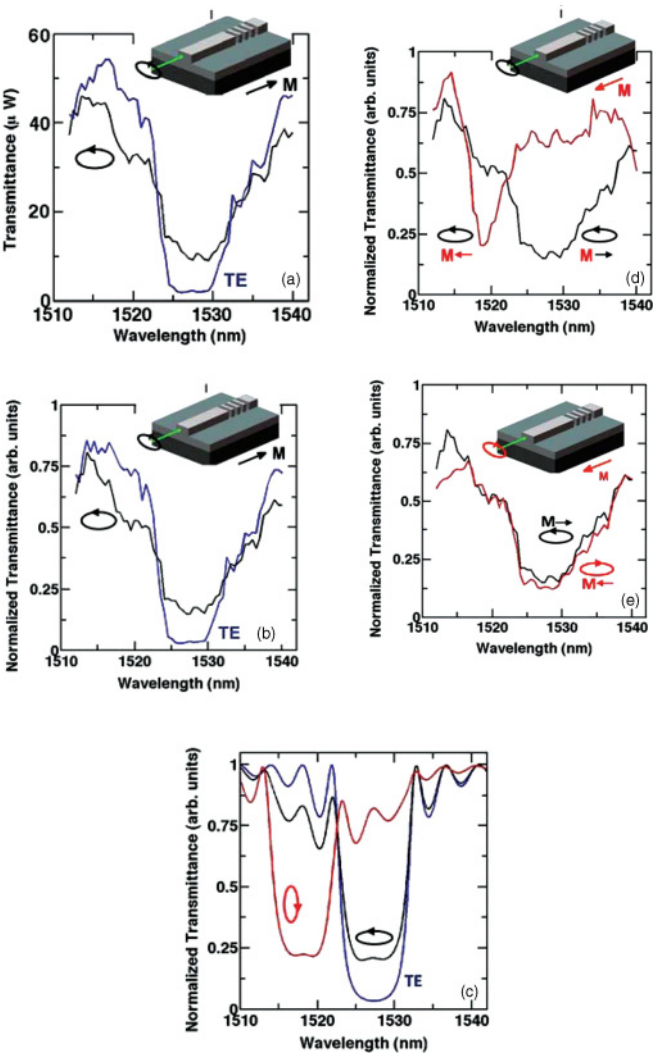

FIG. 6. (Color online) Transmittance profile of fundamental-forward to backward-propagating second-order-mode stop band measured for horizontally oriented semimajor-axis elliptical normal modes in a $Bi_{0.8}Gd_{0.2}Lu_{2.0}Fe_5O_{12}$ film (a) in absolute units and (b) in normalized units to the transmittance of a plain waveguide. The stop band for a TE input in a transverse magnetic field is also shown for comparison. (c) plots the theoretically calculated stop bands for opposite helicity elliptical normal modes. Strong experimentally measured stop band reconfiguration due to mode conversion is shown in (d) for a reversed-helicity mode (not normal) stop band (red). (e) plots the stop band for simultaneous helicity and magnetization reversal.

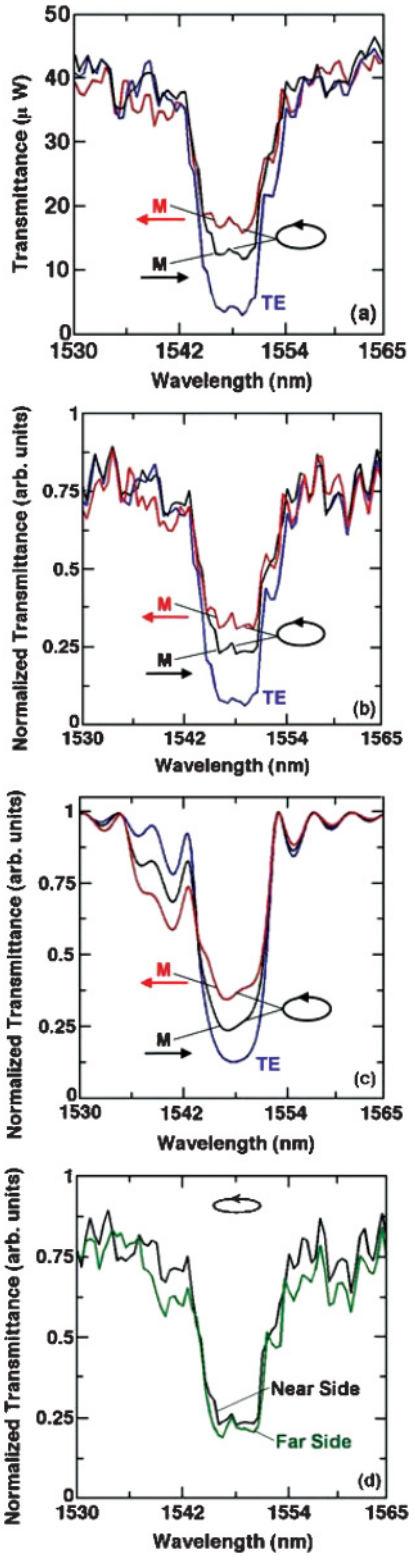

FIG. 7. (Color online) Bloch mode reconfiguration is experimentally shown in (a) absolute units and (b) normalized units through the stop band corresponding to second-order backward propagation for a normal mode and reversed normal mode for a photonic crystal 10 μm away from the input side on the waveguide. (c) Theoretical calculations confirm the Bloch mode reconfiguration. (d) plots the stop bands from the far-side (green curve) and near-side facet (black curve).

C. Stop band spectra and Bloch mode reconfiguration upon magnetization reversal

The effect on stop band reconfiguration as a result of Bloch mode reconfiguration upon magnetization reversal is studied experimentally through launching the normal mode from the near side of the magnetophotonic crystal structure. We compare these results with stack model calculations for the asymmetric scattering from forward-fundamental mode to backward-propagating second-order mode for photonic crystals with period 345 nm patterned on $Bi_{0.8}Gd_{0.2}Lu_{2.0}Fe_5O_{12}$ 2.7-μm-thick films.

Upon magnetization reversal, polarization modifications of the coupled input light in the small feeder section of less than 10 μm (Fig. 4) are minimal. The polarization state of the mode entering the Bragg grating can therefore be assumed to be essentially unchanged in helicity and ellipticity by the magnetization reversal. However, a comparison of the experimental transmittance for forward- (normal mode) and backward-pointing magnetization (not normal mode) in Fig. 7 shows that the transmittance inside the stop band increases. These results are reproducible and real, though not very large. We ascribe these changes to normal mode helicity reversal as these reversals impact the coupling strength of the elliptically polarized input and hence the transmittance.

Theoretical calculations Fig. 7(c) based on the model described in Sec. II agree very well with these measurements. Bloch mode reconfiguration as a result of magnetization reversal is due to helicity reversal of the local normal modes in the photonic crystal. This reconfiguration impacts the coupling of the input polarization to the Bloch state and hence the transmittance. Forward-propagating modes, but especially back-reflected high-order modes exhibit strong elliptical anisotropy and impact the transmittance upon helicity reversal. Magnetization reversal rotates the local polarization vectors $\hat{e}^{f,b}_{+,-}$ affecting the back reflection, even if the input polarization and its helicity are not altered. This reconfiguration reduces the coupling to the back-reflected modes inside the stop band, as shown in Fig. 7.

Figure 7(d) plots the transmittance spectra of a horizontal normal mode upon coupling from the near and far sides of the photonic crystal, respectively. Clearly, the normal-mode transmittance spectra from both sides of the photonic crystal coincide, except for small deviations on the side wings. We ascribe these to mode conversion effects from fiber mode to waveguide mode on the near side and to small semimajor axis reorientations in the feeder section on the far side. It should be noted that Bloch mode reconfiguration affects the center stop band and is not due to mode conversion effects.

V. CONCLUSION

The key finding here is that magnetization and helicity reversals induce a change in the stop band spectral shape in elliptically birefringent gyrotropic photonic crystals. This change is caused by the transmutation of the normal into nonnormal modes and the reconfiguration of Bloch modes upon magnetization reversal. The effect is very pronounced for asymmetric back reflection between different-order modes in multimode photonic crystals. In the waveguide feeder

section, the very same polarization state changes character upon magnetization reversal, and this change of character is the cause of the stop band retuning. No longer being a normal mode upon magnetization reversal, the mode breaks up into other normal modes that propagate with different effective indices and produce a different transmittance response. In the photonic crystal itself, magnetization reversal brings about a change in the helicity of the local normal modes resulting in stop band reconfiguration even when the input polarization maintains its helicity and ellipticity. The large spectral detuning for high-order mode asymmetric contradirectional coupling presented here may be applicable to fast on-chip optical switching devices.

ACKNOWLEDGMENTS

This material is based upon work supported by the National Science Foundation under Grant No. 0856650. All films for this study were grown at Integrated Photonics, Inc. The authors thank V. J. Fratello for the LPE films.

*mlevy@mtu.edu

[1] M. Inoue, K. Arai, T. Fuji, and M. Abe, J. Appl. Phys. **83**, 6768 (1998).
[2] M. Steel, M. Levy, and R. M. Osgood, J. Lightwave Technol. **18**, 1297 (2000).
[3] S. Kahl and A. M. Grishin, Phys. Rev. B **71**, 205110 (2005).
[4] A. B. Khanikaev, A. V. Baryshev, A. A. Fedyanin, A. B. Granovsky, and M. Inoue, Opt. Express **15**, 6612 (2007).
[5] A. Figotin and I. Vitebsky, Phys. Rev. E **63**, 066609 (2001).
[6] A. Figotin and I. Vitebsky, Phys. Rev. B **67**, 165210 (2003).
[7] M. Vanwolleghem, X. Checoury, W. Smigaj, B. Gralak, L. Magdenko, K. Postava, B. Dagens, P. Beauvillain, and J. M. Lourtioz, Phys. Rev. B **80**, 121102(R) (2009).
[8] F. Wang and A. Lakhtakia, Phys Rev. B **79**, 193102 (2009).
[9] F. D. M. Haldane and S. Raghu, Phys. Rev. Lett. **100**, 013904 (2008).
[10] Z. Wang, Y. D. Chong, J. D. Joannopoulos, and M. Soljačić, Phys. Rev. Lett. **100**, 013905 (2008).
[11] Z. Wang, Y. Chong, J. D. Joannopoulos, and M. Soljačić, Nature **461**, 772 (2009).
[12] T. Murzina, R. V. Kapra, T. V. Dolgova, A. A. Fedyanin, O. A. Aktsipetrov, K. Nishimura, H. Uchida, and M. Inoue, Phys. Rev. B **70**, 012407 (2004).
[13] M. Levy, H. Yang, M. Steel, and J. Fujita, J. Lightwave Technol. **19**, 1964 (2001).
[14] M. Levy and R. Li, Appl. Phys. Lett. **89**, 121113 (2006).
[15] R. Li and M. Levy, Appl. Phys. Lett. **86**, 251102 (2005).
[16] X. Huang, R. Li, H. Yang, and M. Levy, J. Magn. Magn. Mater. **300**, 112 (2006).
[17] M. Levy and A. A. Jalali, J. Opt. Soc. Am. B **24**, 1603 (2007).
[18] M. Levy, J. Appl. Phys. **99**, 073104 (2006).
[19] M. Levy, A. A. Jalali, Z. Zhou, and N. Dissanayake, Opt. Express **16**, 13421 (2008).
[20] A. A. Jalali and M. Levy, J. Opt. Soc. Am. B **25**, 119 (2008).
[21] A. M. Merzlikin, M. Levy, A. A. Jalali, and A. P. Vinogradov, Phys. Rev. B **79**, 195103 (2009).
[22] N. K. Dissanayake, M. Levy, A. A. Jalali, and V. J. Fratello, Appl. Phys. Lett. **96**, 181105 (2010).
[23] Z. Wu, M. Levy, V. J. Fratello, and A. M. Merzlikin, Appl. Phys. Lett. **96**, 051125 (2010).
[24] G. Alagappan, X. W. Sun, P. Shum. M. B. Yu, and M. T. Doan, J. Opt. Soc. Am. B **23**, 159 (2006).
[25] K. Busch and S. John, Phys. Rev. Lett. **83**, 967 (1999).
[26] E. P. Kosmidou, E. E. Kriezis, and T. D. Tsiboukis, IEEE J. Quantum Electron. **41**, 657 (2005).
[27] D. McPhail, M. Straub, and M. Gu, Appl. Phys. Lett. **86**, 051103 (2005).
[28] F. Wang, A. Lakhtakia, and R. Messier, J. Mod. Opt. **50**, 239 (2003).
[29] A. Figotin, Y. A. Godin, and I. Vitebskiy, Phys. Rev. B **57**, 2841 (1998).
[30] H. Takeda and K. Yoshino, Phys. Rev. B **67**, 245109 (2003).
[31] C. Xu, X. Hu, Z. Li, X. Liu, R. Fu, and J. Zi, Phys. Rev. B **68**, 193201 (2003).
[32] H. Chen, C. T. Chan, S. Liu, and Z. Lin, New J. Phys. **11**, 083012 (2009).
[33] K. Yoshino, Y. Shimoda, Y. Kawagishi, K. Nakayama, and M. Ozaki, Appl. Phys. Lett. **75**, 932 (1999).
[34] W. Park and J. B. Lee, Opt. Photonics News **20**(1), 40 (2009).
[35] A. E. Serebryannikov and A. Lakhtakia, J. Opt. Soc. Am. B **27**, 2151 (2010).
[36] J. H. Wu, L. K. Ang, A. Q. Liu, H. G. Teo, and C. Lu, J. Opt. Soc. Am. B **22**, 1770 (2005).
[37] C. D. Stanciu, F. Hansteen, A. V. Rimel, A. Kirilyuk, A. Tsukamoto, A. Itoh, and Th. Rasing, Phys. Rev. Lett. **99**, 047601 (2007).
[38] B.E.A. Saleh and M.C. Teich, *Fundamentals of Photonics* (Wiley-Interscience, New Jersey, 2007), pp. 229–230.
[39] H. Nishihara, M. Haruna, and T. Suhara, *Optical Integrated Circuits* (McGraw-Hill, New York, 1985), pp. 65–68.
[40] B. Schaefer, E. Collett, R. Smyth, D. Barrett, and B. Fraher, Am. J. Phys. **75**(2), 163 (2007).